SYNTHESIS AND SINTERING 4 (2024) 87–100

Available online at www.synsint.com

Synthesis and Sintering

ISSN 2564-0186 (Print), **ISSN** 2564-0194 (Online)

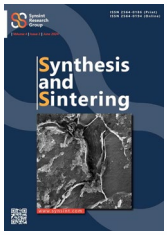

Review article

Additive manufacturing of AISI 304L stainless steel: A review of processing parameters and mechanical performance

Aliasghar Abouchenari [a,*], **Mohamad Javad Jalilpour** [b], **Mohammad Reza Ahmadpour Yazdi** [c]

[a] *Department of Materials Engineering, Shahid Bahonar University, Kerman, Iran*
[b] *Department of Civil Engineering, Kharazmi University, Tehran, Iran*
[c] *Department of Materials Science and Engineering, Sharif University of Technology, P.O. Box 11365-9466, Tehran, Iran*

ABSTRACT

Additive manufacturing (AM) has become a favorable method for producing 304L stainless steel (SS) for various industrial applications, which is owing to its favorable characteristics including corrosion resistance, mechanical performance, and design flexibility. This review paper presents a comprehensive overview of the processing factors along with the mechanical performance of AM-fabricated 304L SS (AM304LSS). Firstly a discussion is provided for the fundamental principles of AM techniques that are common for processing SS304L. This includes selective laser melting (SLM), laser beam powder bed fusion (LB-PBF), direct metal laser sintering (DMLS), directed energy deposition (DED), wire-and-arc additive manufacturing (WAAM). Subsequently, the impact of key processing factors i.e. laser power, and powder characteristics on the microstructure and mechanical properties of AM304LSS is presented. In addition, this article examines recent progress in process optimization strategies and post-processing techniques for improving and enhancing the mechanical properties and surface finish of AM 304L stainless steel components. Finally, significant insights are provided for researchers, engineers, and practitioners involved in the advancement and application of AM304LSS components.
© 2024 The Authors. Published by Synsint Research Group.

KEYWORDS

Direct metal laser sintering
304L stainless steel
Selective laser melting
Directed energy deposition (DED)
Three-dimensional printing

OPEN ACCESS

1. Introduction

Additive manufacturing (AM) of metallic components possesses a series of methodologies involving the synthesis and fabrication of objects in a layer-by-layer approach based on a 3-dimensional (3D) model (Fig. 1). The experimental AM system set-up as well as the powder feeder in the AM process is presented in Fig. 2. As it is clear, the device is a three-axis system equipped with a high-power diode laser of Gaussian-type beam profile. Argon and nitrogen gases are employed for shielding and powder feeding rates, respectively. The nitrogen as powder-feeding gas is vital for delivering metallic powder to the melt pool. This is performed through a specialized three-way powder conveying pipe integrated into the additive head. Also, a powder feeder system is used to provide precise control over the powder feed rate. This is vital for maintaining process stability and quality. The three-axis stage of the AM device provides a travel distance of 50 × 50 × 30 cm^3 (X, Y, Z axes), which allows for the fabrication of parts having dimensions up to these specifications [1–3]. Compared to alternative manufacturing approaches, AM offers numerous advantages. This enables the production of complex objects [4] that are beyond the capabilities of traditional methods [5]. In addition, the growing complexity of AM components reduces

* Corresponding author. *E-mail address:* aliab596@yahoo.com (A. Abouchenari)
Received 7 May 2024; Received in revised form 20 June 2024; Accepted 21 June 2024.
Peer review under responsibility of Synsint Research Group. This is an open access article under the CC BY license (https://creativecommons.org/licenses/by/4.0/).
https://doi.org/10.53063/synsint.2024.42230

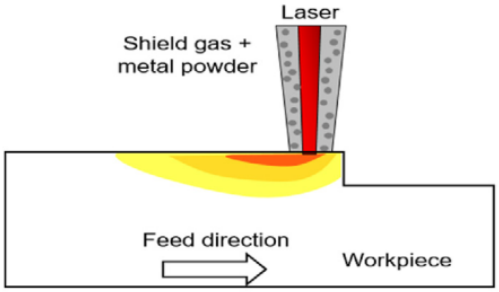

Fig. 1. Schematic illustration of AM process [1].

manufacturing costs. This development brings the industry near to producing components that are topologically optimized, which along with mold elimination, leads to reduced fabrication costs and material losses [6].

The other advantage of the AM process is its capability to customize products across various sectors, such as for prototyping in the industries of aerospace and automotive, as well as in jewelry and biomedical fields, where the production of specific components for special scenarios is essential [7]. Conversely, additive manufacturing requires a significant initial capital investment, particularly for printers of metallic parts which have higher prices than printers of polymers owing to their sophisticated energy and technology demands. Moreover, they exhibit greater sensitivity to the type of metallic powder utilized [6].

Furthermore, 3D-printed metal components exhibit distinct defects that are absent in alternative manufacturing methodologies. The primary issues include the presence of porosity resulting from gaps formed during powder shaping and flow, along with the development of residual stress and extensive grain growth stemming from the diverse consecutive stages of heat treatment, as well as the melting-remelting, induced by the layer-by-layer deposition process [6].

One common prevalent drawback in several AM techniques is the formation of a layered structure throughout the whole synthesized object owing to the fabrication system. These effects have the potential to diminish specific material properties, such as resistance to corrosion along mechanical strength. Various types of metal 3D printing are reported, categorized broadly into powder bed fusion (PBF) and directed energy deposition (DED) fabrication techniques [6].

In the PBF method, a source of energy is utilized to sequentially melt the metallic powder, in the form of layer by layer, within a powder bed. After each layer is sintered or melted, a new powder layer is added onto the bed, and the platform height is lowered for the melting process. An electron beam or a laser or can be utilized in this 3D printing method for metal melting. This approach requires a gas e.g. argon, nitrogen, or a vacuum to preventing metal oxidation. Direct metal laser sintering (DMLS), laser powder bed fusion (LPBF), and selective laser melting (SLM) are examples of PBF methods [6].

Fusion and powder deposition occur simultaneously in the DED process, which is commonly facilitated by a laser. The melted material is deposited onto a substrate that can be repositioned along certain axes. Similar to PBF, this process also necessitates an inert gas to prevent oxidation. Wire Arc Additive Manufacturing (WAAM) is considered an instance of the DED method [6].

Despite the abovementioned advantages, the DED procedure is characterized by low powder effectiveness and results in a final rough surface that typically requires machining post-fabrication. Previous evaluations have demonstrated that the thermal history of a piece synthesized through DED significantly affects its microstructure and mechanical properties [8–10]. Consequently, the quality of components produced by DED is primarily dictated via the parameters employed throughout the fabrication technique. Notably, DED allows for the adjustment of numerous parameters including scan speed, laser power, building atmosphere, powder feed rate, deposition pattern, etc. [11].

Stainless steels (SSs) are among the main extensively researched metallic alloys in AM owing to their capacity to efficiently produce complex components compared to traditional manufacturing techniques [12, 13]. SSs comprise multiple grades based on their chemical composition, where the microstructural characteristics evolve with varying alloying elements like chromium, nickel, manganese, niobium, and molybdenum [14]. A notable example is the austenitic SS304L, known for its robust strain hardening ability attributed to twinning-induced plasticity (TWIP) as well as transformation-induced plasticity (TRIP) resulting from its low stacking fault energy (SFE) relative to other commercial stainless steels [15]. Researchers have observed hardening behaviors of TWIP and TRIP in AM304LSS due to its low

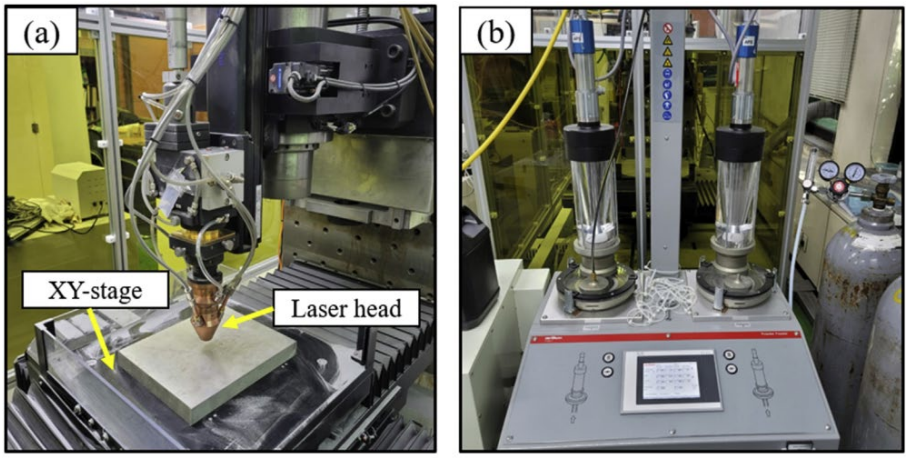

Fig. 2. a) AM process and b) powder feeder experimental set-up [1].

SFE, with the TRIP phenomenon being suppressed in DED-fabricated 304L stainless steel and enhanced in SLM-fabricated 304L stainless steel [13, 16, 17].

2. Applications of 304L stainless steel

Austenitic SSs have found widespread applications in industries i.e. chemical parts, petrochemical units, and power generation as a result of the ability their show in facing high-temperature creep even under stresses exceeding the yield point. Among the austenitic group, type 304 SS stands out as the most commonly utilized alloy [18].

The alloy known as type 304L exhibits a diverse fundamental type 302 or 18-8 grade, featuring increased Cr levels and reduced carbon (C) content. The diminished C content serves to minimize both the precipitation of Cr-carbides due to welding as well as its susceptibility to intergranular-type corrosion. Also, in numerous cases, this alloy can be utilized in the 'as-welded' state, whereas type 302 necessitates annealing to uphold satisfactory corrosion behavior. Type 304L represents an ultra-low-C version of type 304, characterized by a maximum C content of 0.03%, thereby avoiding precipitation of carbides arising from welding [18].

Consequently, this particular alloy could be applied in the “as-welded” state, even when subjected to severe corrosive environments. Type 304 shows somehow higher mechanical properties compared to type 304. The sustained exposure temperature limit for types 304 and 304L, avoiding notable scaling, stands at approximately 900 °C. In cases of intermittent exposure, the highest temperature for exposure is around 815 °C. Heat treatment for hardening is not applicable for type 304L. Annealing of this alloy would be performed within a temperature in the range of 1040 to 1120 °C, followed by quenching. Stress relief for cold-worked components can be carried out at 400 °C for half to two hours [19]. A significant portion of small-diameter seamless pipes utilized in superheaters and heat exchangers are produced through cold drawing or cold-forming techniques; hence, a comprehensive examination of the creep and mechanical performance of cold-drawn SS304L is imperative [18].

The scope of applications for 304L encompasses a wide range of sectors from nuclear reactor parts to chemical machinery and the oil industry [20, 21]. The utilization of SS304L extends across diverse engineering and household appliance domains. Noteworthy applications of SS304L encompass aerospace, automotive, culinary equipment, petrochemicals, and food processing apparatus, among others, where resistance to corrosion and heat are pivotal considerations [22]. Additionally, 304L emerges as a promising candidate for serving as a matrix in steels with an oxide dispersion-strengthened (ODS) mechanism, at which nanoparticles (NPs) of oxides are distributed throughout the SS304L base [23].

Bait et al. [24] declared that SS304L can be used in biomaterials applications. They explored the impact of the bias voltage of substrate on the characteristics of titanium dioxide (TiO_2) coatings deposited via radio-frequency magnetron sputtering on an SS304L. They compared the corrosion resistance levels of coated and uncoated specimens. They observed a reduction in the current density of corrosion for the coated counterparts.

Yeom et al. [25] conducted a feasibility assessment of the cold spray deposition technique involving SS304L onto 304 SS substrates as a strategy for mitigating Cl-induced stress corrosion cracking (CISCC) under varied substrate conditions. CISCC has the potential to manifest in or around the fusion-welded zones of SS containers within dry cask storage systems designated for utilized nuclear fuel. The outcomes of their study indicated that utilizing a cold-sprayed SS coating proved to be a feasible choice for establishing a physical barrier against CISCC in fusion weld zones of SS within aggressive chloride salt-bearing environments.

3. AM technologies for AISI 304L stainless steel

3.1. Powder bed fusion approach

The PBF approach is a manufacturing method that encompasses the application of a layer of powdered plastic or metal material, onto a construction platform. It is possible to categorize it into LPBF, generally recognized as SLM (or direct metal laser melting (DMLM)), (Fig. 3a) when a high-energy laser is employed to fuse the powder or electron beam powder bed fusion (Fig. 3b) if an electron beam is utilized to selectively melt the powder, merging it to form a solid layer. Next, this procedure is iterated, incorporating more powder layers that are melted since the final component is achieved [26].

3.2. Selective laser melting (SLM)

In SLM, a laser with high-power density is utilized to fuse and melt metallic powders in a bed. A melting-remelting of the powder is occurred. This technique makes it possible to fabricate near-net-shape objects with advanced mechanical properties and almost full densities. Several factors may control SLM, e.g. the infill orientation, building direction, or scan speed [6, 27].

The LPBF technique employs high-powered lasers to melt and then solidify layers of metallic powder arranged on the work surface [28], following the computer-aided design model. The laser scanning methodology, inert atmosphere, layer thickness, speed and power, and several other factors are determined by the operator and need to be optimized according to the materials and system employed [29]. Despite SLM’s reputation for generating fully dense elements with remarkable accuracy in an almost short timeframe, the process of production is rather costly and is exclusively suitable for industries dealing with high-value parts, at which enhanced performance could lead to cost savings, such as the aerospace industry [26, 30].

3.3. Directed energy deposition (DED) technology

Lately, another approach utilizing SS304L for synthesis and manufacturing parts through AM is DED, which, despite utilizing an electron beam or laser, differs from powder bed methods as the material is either wire or maybe powder that is directly located onto the object (Fig. 4). Multi-axis nozzles are utilized in DED to move metal wire or powder to the construction plane and an electric arc or laser is used to melt/fuse it [31, 32]. The advantages of DED lie in the fabrication of big specimens or the restoration of existing ones [26]. An illustration of this process is depicted in Fig. 4 [33].

Moreover, it is important to note that various terminologies are commonly utilized in the literature to refer to this process [34]. An outline of these terms is detailed in Table 1 [33]. In particular, the DED approach is affected by many process parameters including laser parameters and powder characteristics. In this regard, Shin et al. [35] conducted an experiment to obtain the conformity criterion of the DED technique for metallic powder (SS304L). Firstly, they investigated the

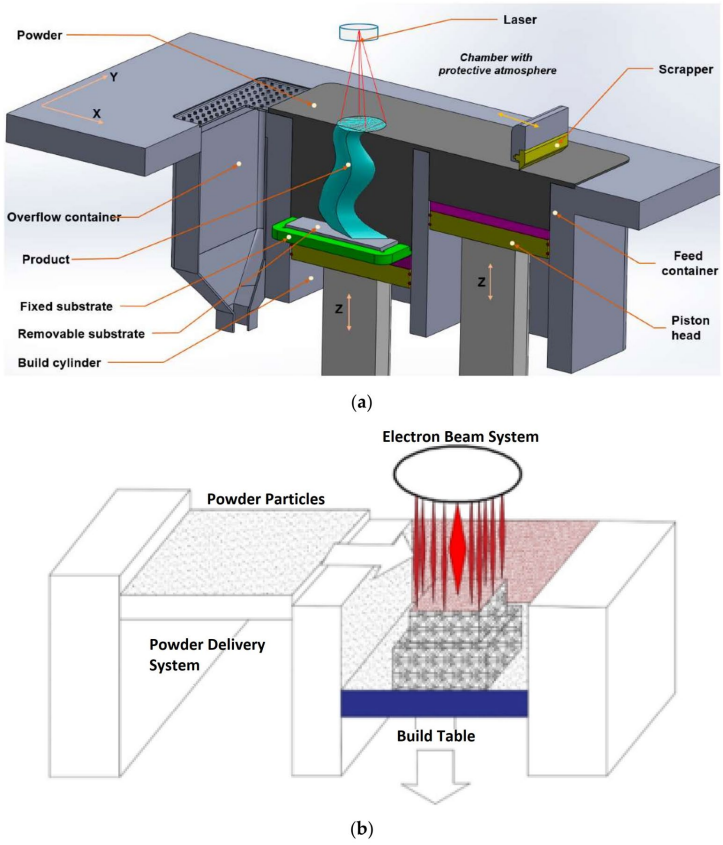

Fig. 3. a) SLM technology and b) EBM technology [26].

effects of powder feed rate, moving speed of laser header, laser energy output, and rate of gas feeding on the DED technique. Their results depicted that as the laser header moved faster the deposition height decreased and that the width and the dilution ratio of the heat-affected zone (HAZ) highly depend on the powder feed rate and laser power. They also declared that conventional SS304L casting samples showed a tensile strength of about 500 MPa, although deposition specimens fabricated via a metal DED 3- dimensional printing process depicted a better tensile strength of 625 MPa.

3.4. Wire-and-arc additive manufacturing (WAAM)

Several other methodologies exist for the printing of AISI 304L SS, such as the WAAM process [36, 37], each presenting distinct advantages and drawbacks concerning the resultant quality in terms of microstructure [38], mechanical performance, and the residual stresses owing to fusion procedures [26]. Ji et al. [39] synthesized SS304L parts using WAAM and characterized their microstructure and mechanical characteristics (Fig. 5).

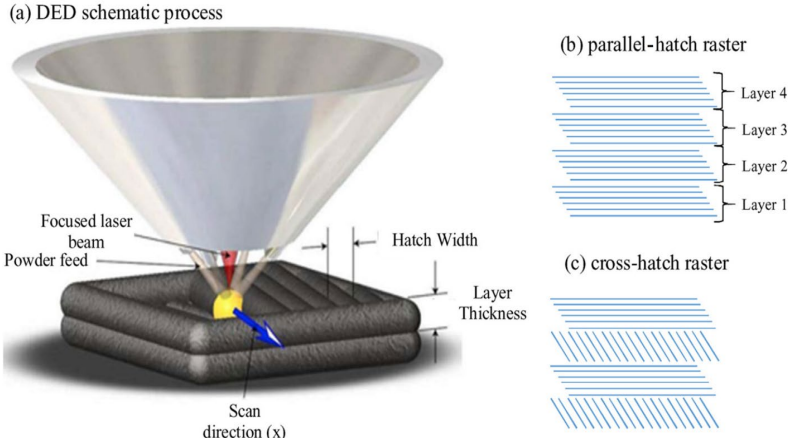

Fig. 4. Schematically illustration of the DED technique a) wherein a focused laser beam melts the sprayed SS powder onto the part. Standard laser raster patterns: the location of the powder deposited in a b) x-parallel-hatch, and c) x-cross raster [33].

Table 1. Various DED processes commercialized names [33].

Acronym	Technology
LMD	Laser metal deposition
LENS	Laser energy net shaping
LAMP	Laser-aided manufacturing process
DMD	Direct metal deposition
LPF	Laser powder fusion
DLF	Direct laser fabrication

They developed the WAAM system which significantly consisted of a computer, a wire feeder, the working chamber as well as the GTAW apparatus (Fig. 6a). A melting source is utilized to melt the wire, and the whole environment is filled with argon-inert gas. The WAAM physical picture is illustrated in Fig. 6b [39].

They observed dendritic microstructures with varying morphologies and spacing, influenced by processing parameters. The growth direction of these dendrites follows the temperature gradient. Notably, dendrite morphology evolves from fine and messy at the bottom layers to large and stable at the top layers. They also declared that similar to other AM processes, anisotropy is a mechanical property that indicates how the grain boundary strengthening varies in various directions (Table 2) [39].

Meanwhile, the accuracy of the products fabricated via WAAM is reduced due to severe heat accumulation, which in turn deteriorates its mechanical properties and microstructure. Due to its weak heat dispersion, it is harder to get complex SS components with WAAM compared with common SS304L. One can efficiently reduce the heat accumulation, via a water-medium active cooling AM apparatus to finish a SS304 with a thin-walled design. Consequently, taller and narrower thin-walled specimens would be fabricated that have a 13% decrease and a 7% increase in average width and height, respectively. Along with this, the waviness of the surface is also mitigated, the fracture performance of thin-walled parts is developed and grains are refined [41].

3.5. Comparison of AM techniques for processing 304L stainless steel

Various laser-based additive manufacturing (AM) processes, including LPBF, DMLS, SLM, and DMLM, have diverse benefits and results when processing 304L stainless steel. Although these methods are similar, the main distinction between them is whether or not the metal powder is completely melted during the manufacturing process. A comparison of tensile strength, UTS, and elongation of samples fabricated via different 3D-printing methods for SS304L is presented in Table 3.

Instead of completely melting the metal powder, direct metal laser sintering (DMLS) concentrates on sintering it. This process can affect the end product's attributes, frequently producing pieces that don't have the same density or mechanical qualities as those made by complete melting procedures. Because of this, DMLS can be used with materials that are heat-sensitive or with certain specialized uses.

On the other hand, methods where the metallic powder is completely melted by the laser are referred to as DMLM, LPBF, and SLM. Parts made using this full melting method typically have characteristics more in line with conventionally fabricated metal components. When these technologies are used instead of sintering processes like DMLS, the components that are created usually have better mechanical qualities and a higher density. As a result, SLM, LPBF, and DMLM are frequently used for materials that benefit from the full melting process to obtain ideal performance characteristics and for applications requiring high-strength, high-density components.

Therefore, the choice of technique relies on the special demands of the application, including the desired mechanical properties, material characteristics, and functional demands of the final product. While DMLS offers advantages for specific applications and materials that are difficult to melt, SLM, LPBF, and DMLM provide advantages in producing higher-density and mechanically robust parts.

4. Processing parameters and their influence on AM304LSS microstructure and mechanical performance

In this section, we explore the processing parameters and their outcome on the microstructure and mechanical behavior of AM304LSS. Key parameters like laser power, speed of scanning, layer thickness, powder characteristics, and the use of an inert gas atmosphere are critically discussed. These factors significantly impact the resulting tensile strength, fatigue behavior, hardness and wear resistance, impact toughness, and corrosion resistance of the fabricated material. Understanding how each parameter affects the microstructure enables optimization of the manufacturing process to achieve desired mechanical properties and performance in various applications.

Lee et al. [48] conducted a comparative analysis of the resistance to hydrogen embrittlement in conventionally and austenitic AM304LSSs. Surprisingly, no substantial variation in the level of deformation-induced α′-M between the CA-TMT and LPBF specimens was noted. This indicates that the solidification substructure promoted the strength

Table 2. A comparison of the 304L and SS304L mechanical performance produced through the AM and forging processes.

AM technique	SS	Orientation	YS (MPa)	UTS (MPa)	EL (%)	Ref.
LMD	304L	Transverse	338	609	48.2	[13]
		longitudinal	314	606	56.4	
SLM	304	Transverse	535	693	41.8	[19]
		longitudinal	455	580	57.5	
WAAM	304L	Transverse	235	680	55.5	[39]
		longitudinal	230	620	88.0	
Forged	304L		≥ 170	≥ 480	≥ 40	[40]

of the LPBF specimen without enhancing the detrimental embrittlement effects of hydrogen [48].

Somewhere else, Lee et al. [49] made an examination of the role of the roughness of the surface on the fatigue failure of AM304LSS, focusing on both machined/polished and as-built surface conditions. Their findings revealed that while surface roughness exhibited some locational dependency related to the part position on the build plate relative to the inlet of inert gas, this effect was not statistically significant. They identified that in the elevated cycle fatigue regime, the initiation of cracks in as-built samples was influenced by surface characteristics. This results in early fatigue failure. In contrast, for machined/polished specimens, cracks are typically initiated at or near surface defects. Surface roughness sensitivity varied with the loading condition, being lower under strain-based loading but significant under stress-based loading, especially at lower stress levels. Lee et al. [49] concluded that standard surface roughness parameters, ultimate tensile strengths (UTS), notch sharpness, grain size, and smooth surface endurance limit can effectively predict the fatigue life for stress-life behavior. For strain-based fatigue loading, a typical surface factor technique was found adequate, with predictions falling within a reasonable scatter range from experimental results [49].

In the study by Sehhat et al. [47], the mechanical performance of components synthesized with water- and gas-atomized SS304L powder in the LPBF process was compared. They found that parts made fromgas-atomized powder showed remarkably elevated yield tensile strength (YTS) and EL in comparison with those made from water-atomized powder. Nevertheless, their UTS were similar. This suggests that powder characteristics, particularly the method of atomization, play a crucial participation in determining the mechanical properties of the obtained parts manufactured by the LPBF approach.

Hawk et al. [50] explored the spot-welding behavior of AM304LSS compared to wrought 304L stainless steels. They found differences in the resulting spot weld microstructures, with additively manufactured welds containing both cellular austenite and massive austenite, unlike the fully austenitic welds of wrought 304L. These differences were attributed to variations in composition and solidification rates between the two types of materials.

Table 3. Tensile strength, UTS, and EL of samples produced via different 3D-printing methods for 304L stainless steel.

Additive manufacturing method	Tensile strength (MPa)	UTS (MPa)	Elongation (%)	Ref.
SLM	427	596	41.5	[42]
	541	694	39	[19]
DED	320	620	72	[43]
	480–420	600–700	70	[44]
WAAM	~300	~510	-	[45]
	~300	700	50–65	[46]
LB-PBF via gas atomized water atomized	507	688	0.69	[47]
	470	674	0.29	

Krentz et al. [51] discovered that the baseline tensile strength and fracture failure of AMed 304L and 316L stainless steel samples were comparable to those of wrought materials. Additionally, the hydrogen properties of the additively manufactured specimens exhibited similar properties to wrought materials, indicating the potential for high-quality AM parts.

Sutton et al. [52] performed an investigation into the role of several reuses of AISI 304L SS powder in the LPBF process. Their outcomes showed that recycled powder became more spherical, coarsened, and accrued oxygen, which led to improved flowability. The accumulation of delta ferrite was also observed with successive recycling. This indicated changes in the powder's morphological properties and chemical composition over time.

The influence of build orientation and heat treatment on the phase transformation of martensite (M) in AM304LSS was studied by Ferreri et al. [53], revealing that M transformation rates were lowered for AM parts treated at temperatures about 1100 °C. Above this temperature, recrystallization occurred, which increased the rate of M transformation for the specimens treated at elevated temperatures.

Zhang et al. [54] investigated the relationship between the thermal stability of cellular substructures (CSs) in AM304LSS and inclusion interface evolution. They showed that high annealing temperatures induced a transformation in the inclusion types. This affected the interfacial properties and, consequently, the thermal stability of the CSs. They concluded that the semi-coherent interface between the inclusions i.e. $MnSiO_3$ and the matrix of LPBF SS304L played a significant role in maintaining high ductility and strength.

Ghayoor et al. [55] focused on the thermal stability of LBPF AM304LSS oxide dispersion strengthened (ODS) alloy. Their findings indicated that although dislocations were annihilated, the LPBF approach still partially maintained the induced cellular substructure even after aging at approximately 1200 °C. The presence of Y-Si-O NPs hindered recrystallization and grain growth, leading to enhanced yield stress (YS) and creep properties compared to wrought SS304L.

The thermal stability of dislocation cellular structures was studied by Deng et al. [56] in various AMed austenite-containing SSs. They found that minor alloying elements i.e. Al and Mo significantly affected the stability of these structures. Also, the AM 316L SS showed the highest stability because of Molybdenum segregation at cellular walls, whereas AMed 316L(Al) SS exhibited the lowest stability due to its high SFE.

Studies on SLM of SS304L have provided valuable perspectives about the microstructure, residual stresses, and mechanical and fatigue performance of the obtained parts. Researchers have elucidated the vital role of processing parameters and their effects on material performance through various investigations.

Zhang et al. [57] performed an extensive examination of the microstructure and fatigue performance of SLMed SS304L. They found that SLMed SS304L shows fascinating fatigue behavior at high stress levels. The study highlighted the role of laser power and scanning speed on surface roughness and porosity. They emphasized the importance of optimizing these parameters to enhance fatigue resistance.

Another crucial aspect of SLMed parts called residual stress, was examined by Zhang et al. [57]. They proposed a theoretical model to explain residual stress relaxation during base plate removal. They observed a linear relationship between residual stress and energy density. This indicated the potential for controlling residual stresses through process parameters.

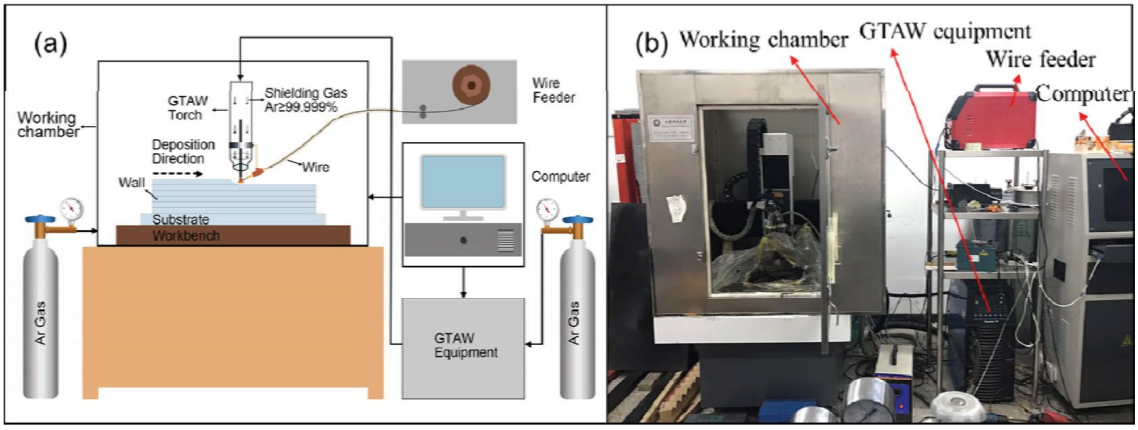

Fig. 5. a) Schematic illustration of the experimental setup developed by Ji et al. and b) WAAM system [39].

Fatigue failure mechanisms were also investigated by Zhang et al. [57]. They identified fatigue crack initiation as the primary factor that affects fatigue performance. They introduced a 'critical' value to determine the remarkable role of surface roughness and porosity. They highlighted the importance of managing these factors to improve the fatigue life. They also explored the role of local recrystallization performance on fatigue behavior and revealed that strain-sensitive regions (SSRs) act as preferential nucleation sites for fatigue cracks. They in turn, significantly reduce the fatigue performance in parts with low porosity. Moreover, their study focused on the importance of eliminating SSRs to enhance fatigue resistance [57].

Nguyen et al. [58] focused on the impact of laser power on the fatigue life cycles and microstructure of SLM-fabricated SS304L. They demonstrated that low laser power led to irregular defects and reduced fatigue lifetime, while unique microstructures enhanced energy dissipation during cyclic deformation. This in turn contributes to improved fatigue resistance of components.

Zhang et al. [59] conducted tensile and fatigue tests on SLMed SS304L to evaluate the role of laser power in determining fatigue performance. They found that low laser power resulted in irregular defects, that lead to stress concentration sites and reduced fatigue lifetime. Moreover, detailed microstructural characterizations revealed unique heterogeneous microstructures in SLMed SS304L. This enhances the working performance during tensile deformation and contributes to improving fatigue resistance compared to conventional materials.

Furthermore, Tomanek et al. [60] observed the impact of porosity on the electrical, thermal, and mechanical properties of SLMed SS304L. They observed degradation in these properties especially mechanical performance with increasing porosity. This highlights the importance of minimizing porosity to maintain material integrity.

Zhang et al. [61] focused on enhancing fatigue resistance through a unique heterogeneous microstructure in AM304LSS. Their findings highlighted the crucial role of CSs in regulating dislocation motion throughout the cyclic deformation. This leads to intergranular fatigue cracking along high-angle grain boundaries (HAGBs).

Kim et al. [62] performed an investigation into the relationship between mechanical properties and the dislocation cell structure of AM304LSS. They found that the developed cell networks not only hindered dislocation gliding but also served as pathways for crack propagation throughout the plastic deformation. This resulted in higher strength during tensile testing. The study underscored the significance of dislocation cell structure as a principal mechanism for strengthening AMed materials.

Amine et al. [63] explored the high-temperature microstructure stability

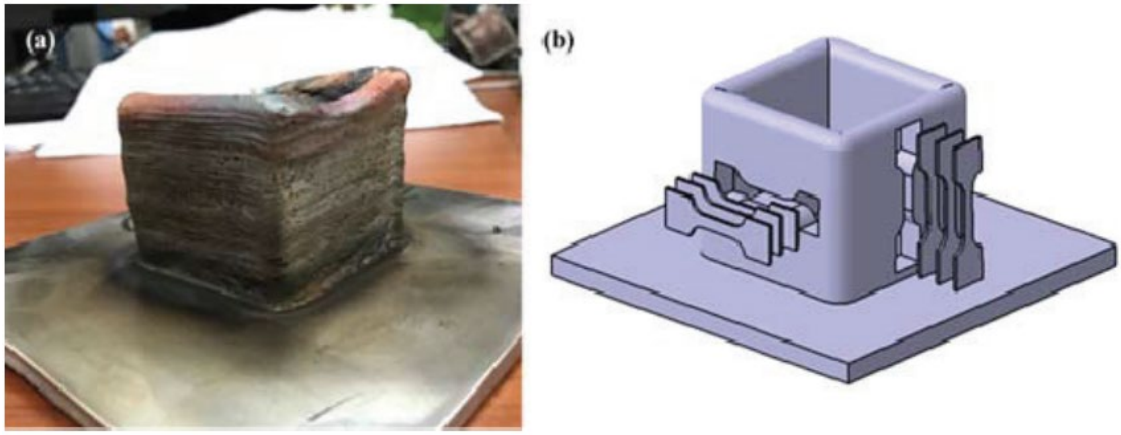

Fig. 6. a) The actual component synthesized by WAAM in the Ji et al. study and b) the schematic illustration of tensile samples extracted from the component [39].

and characteristics of SS304L fabricated via the SLM technique. Their findings revealed the evolution of a cellular structure of austenite and a small quantity of delta-ferrite phase, with remarkable stability observed at track boundaries. Carbide precipitation at grain boundaries during aging affected corrosion resistance. This highlights the importance of understanding microstructural changes under different conditions.

Hung et al. [64] compared the mechanical performance of LFP-manufactured SS304L parts using foils to those fabricated by the SLM approach via powder. They found that LFP parts exhibited improved tensile strength. However, they exhibited lower ductility compared to SLMed parts. The increased strength of LFP parts was ascribed to finer grains resulting from rapid heat dissipation and elevated cooling rates during the LFP approach. Additionally, they observed higher part strength in the horizontal direction for both LFP and SLM parts, with the higher surface area in powder leading to higher contents of oxygen in SLMed parts compared to LFP parts.

Additionally, Pathak et al. [22] focused on the post-processing of SLMed SS-304L using laser shock peening (LSP). Their results demonstrated significant improvements in compressive residual stresses. This highlighted the potential of LSP as a post-processing technique for the improvement of mechanical properties and fatigue behavior of AM parts.

Ghayoor et al. [23] examined the influence of volumetric energy density on the microstructure, mechanical properties, and texture, of SLMed SS304L. They observed a fine cellular substructure across different energy density values, with higher strength and hardness compared to conventionally fabricated SS304L. Heat treatment led to the nucleation of grains with recrystallized equiaxed structure. This influenced the microhardness and the disappearance of the cellular substructure.

Smudde et al. [43] examined the fatigue crack growth rates (FCGR) of DED-produced SS304L. They emphasized the impact of residual stresses compared to conventional wrought materials. They found that DED SS304L exhibited significantly higher near-threshold FCGRs due to tensile residual stress, with rates 3.5 times faster than wrought 304/304L at a ΔK of 5 MPa.m$^{0.5}$. The residual stress intensity factor (K_{res}) for DED samples showed positive values in the range of 4 to 1 MPa.m$^{0.5}$. Meanwhile, wrought materials had negligible residual stress. DED 304L displayed no crack closure effects, unlike wrought materials. This was due to the positive stress ratio and K_{res}. This study brought out the significant influence of residual stress in determining the mechanical and fatigue behavior of DED SS304L, with the unique microstructure of DED materials having a small impact compared to residual stress effects.

Somewhere else, Smudde et al. [65] focused on the effects of residual stress and temperature gradients during DED on orientation-dependent fatigue performance. They investigated how localized heating and resulting temperature gradients create remarkable residual stress that affects the mechanical properties of DED SS304L, particularly in terms of FCGS. This investigation focused on the significant effect of considering residual stress in the evaluation of DED-produced materials.

Fig. 7 illustrates the BSE images depicting the grain size and morphology in the Y-Z plane surrounding the crack path of the DED fabricated SS during horizontal Fig. 7a and vertical Fig. 7b orientations of crack growth. Both micrographs demonstrate a noticeable EL of grains in the build direction (Z) resulting from the induced temperature gradient throughout the DED material deposition. Ultimately, it was determined that the DED material displayed elevated FCGRs relative to wrought samples of identical geometry and test conditions as a function of ΔK_{app} [65].

Smith et al. [44] explored the relationship between fatigue properties and manufacturing defects of DED SS304L. They declared that a large lack of fusion defects (>1 mm) largely reduced ductility, tensile

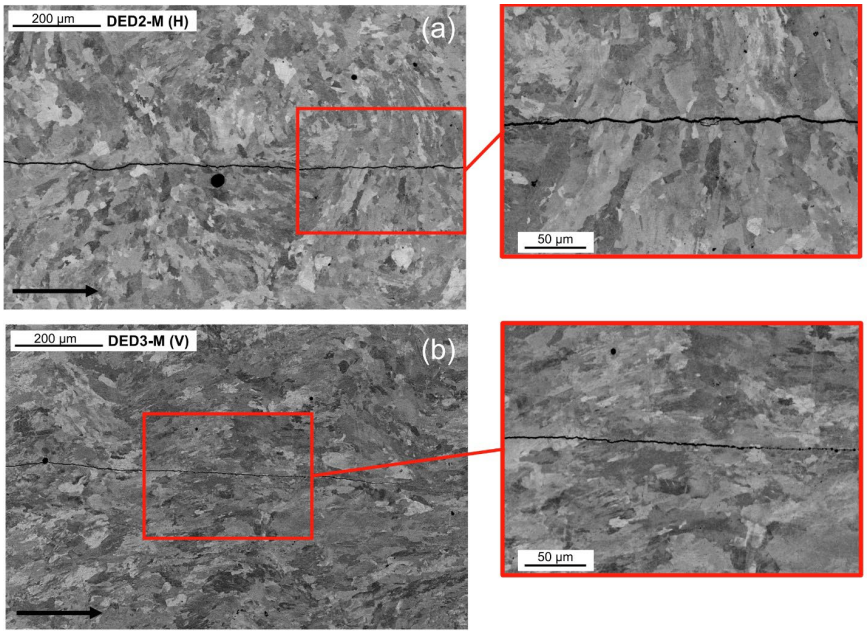

Fig. 7. BSE images of the crack path in DED fabricated parts: a) horizontal and b) vertical crack growth, with black arrows indicating the crack propagation direction [65].

strength, and fatigue life. However, smaller spherical defects had less impact on these properties. The FCGR was less severely affected by defects, indicating only local acceleration proximity of lack of fusion defects. The study suggested that the fatigue life of AMed SS can be normalized by considering the role of defects on UTS, indicating that low defect populations result in fatigue properties similar to those of wrought materials.

Kim et al. [66] focused on the influence of cellular segregation (C.Seg) for high ductility and strength AMed SS304L. Fig. 8 provides a schematic overview of the deformation-induced martensitic transformation (DIMT) approach affected by the C.Seg of AM304LSS. It appears that a cell core exhibiting almost low stability of austenite may experience selective transformation to M since the cell boundaries remain within the austenite phase. Hence, the C.Seg observed in AM304LSS may have facilitated the formation of fine and homogeneous M-phase.

They proposed that element segregation in cellular structures created by dendritic solidification throughout the additive manufacturing approach was seen in the microstructure of undeformed AM304LSS. Comparing AM304LSS to wrought 304L (SS304L), the tensile test revealed higher tensile strength, YS, and even higher EL. Both deformed specimens (AM304LSS and 304L stainless steel) showed deformation-induced M-phase (α'-martensite) following tensile deformation. The deformed SS304L had coarse martensite, whereas the deformed AM304LSS included fine and homogeneous martensite. Interestingly, DIMT to a cellular structure with austenite around the M-phase was seen in deformed AM304LSS. Due to element segregation within cellular structures, the austenite phase region aligned with regions enriched in Ni and the martensite phase region with nickel-depleted parts. This suggests that element segregation altered the stability of the austenite phase and the local chemical composition, which in turn affected the DIMT. It is believed that homogenous martensitic transformation brought about by element segregation in cellular structures of the appropriate scale accounts for the exceptional strength and ductility of AM304LSS [66].

Fig. 9a displays engineering curves of stress-strain derived from AM304LSS and SS304L. Table 4 provides a summary of the related YS, UTS, and EL values. In comparison to the SS304L, the AM304LSS showed a greater YS of ~580 MPa and a higher UTS of ~920 MPa. Furthermore, it was shown that even with the higher tensile strength, the AM304LSS showed notable elongation, with its total elongation of 69% compared to the SS304L's 65%. The frequent occurrence of the M transformation in alloys with DIMT caused a double-yielding pattern in both stress-strain curves [16, 67]. Inflection points on the strain hardening curve, which mark the start of M-phase reorientation and consequent plastic deformation, have been linked to double-yielding behavior [68]. As it is illustrated in Fig. 9a, in the AM304LSS, double yielding was more noticeable [66].

A comparison of the YS, UTS, and EL came from the material studied in this work and AM304LSS is illustrated in Fig. 10a and b [64, 69]. In each graph, dots represent the AM304LSS results extracted from the prior studies. In this investigation, AM304LSS demonstrated a greater strength-ductility combination when compared to the findings found in the literature [66, 70].

McWilliams et al. [71] evaluated the influences of hydrogen on the fracture toughness of LENS AM304LSS. They characterized and compared the LENS AM304LSS in plate form with the forged type 304L. While the YS was more than that of annealed type SS304L, the LENS material revealed lower tensile and yield strengths and EL compared to the forged material.

Fracture toughness tests were performed on forged type and LENS AM304LSS after they were charged with hydrogen. The forged material and AM were both affected by hydrogen. The impact of hydrogen was higher on the Am in comparison to the forged material; AM304LSS toughness was reduced by over 70% as opposed to 60% for the forged. The LENS AMed SS304L fracture surfaces showed microvoid coalescence and ductile fracture properties. Numerous microvoids were found to contain fine silica particles. Periodically, unmelted particles were also seen on the fracture surface [71].

AM304LSS showed reduced ductility but higher yield and tensile strength. In the as-received and hydrogen-charged conditions, the toughness of fracture was less than that of traditionally produced SS304L, but it still meets programmatic applications [71].

Extreme hydrogen environments' impact on the fatigue and fracture performance of AM304LSS was investigated by Smith et al. [72]. They discovered that AM materials with few manufacturing defects showed good tensile strength, ductility, and fatigue resistance under ambient test circumstances, compared with wrought materials. The microstructural characterization revealed that the unique solidification microstructure of AM materials played a significant role in crack propagation under tensile fracture conditions with hydrogen. Nevertheless, the micromechanisms of FCG and tensile fracture were distinct in hydrogen environments. Due to internal hydrogen, powder bed fusion (PBF) and DED 304L with ostensibly identical compositions showed comparable losses in tensile ductility [72].

Wang and Beese [73] examined the impact of chemical composition, i.e. beginning powder chemistry and spatial variations owing to vaporization while manufacturing, on the strain-induced M-phase transformation in DED-fabricated SS304L parts. By mixing pre-alloyed 304L stainless steel powder with powders of iron, they

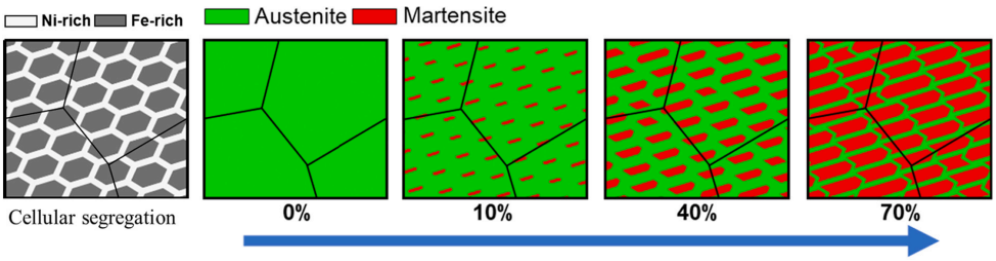

Fig. 8. Schematic illustration of deformation-induced M-transformation as a function of C.Seg of AM304LSS [66].

Table 4. Tensile properties measured for AM304LSS and 304L stainless steel [66].

	YS (MPa)	UTS (MPa)	Total EL (%)
AM304LSS	580	917	70
SS304L	246	670	65

enhanced M phase transformation, leading to increased UTS and EL failure compared to pure DED-deposited 304L walls. The study quantified the variation in chemical composition with the position because of thermal history variations, depicting that austenite stabilizing elements like Ni, Mn, and Cr were preferentially vaporized throughout the deposition. They presented an equation for M transformation kinetics that predicts the change in M-phase volume based on nominal chemistry, strain, and heterogeneous chemistry owing to vaporization in AMed samples [73].

Brown et al. [74] highlighted that AM of metal components leads to distinctive microstructures with distinct mechanical properties compared to conventionally produced components. Their study identified four key microstructural characteristics ascribed to the DED of SS304L: tortuous grain morphology, high dislocation density, local chemical heterogeneity, and increased ferrite content. Using in situ neutron diffraction, they monitored the change in the as-built microstructure throughout the post-build heat treatment and related these microstructural characteristics to the material strength performance. They concluded that the higher flow strength of the AMed material, compared with wrought counterparts, was primarily because of higher dislocation density in the as-built material, with additional strength likely attributed to the unique additive manufacturing grain structure [74].

Nishida et al. [75] elucidated the dynamic mechanical properties of AMed and wrought SS304L under compression and tension for impact applications. Their study found that the flow stress and YS of AM304LSS were higher at low amounts of strains however dropped below those of wrought SS304L at larger strains. This indicated milder work hardening behavior in the additively manufactured material. The AM304LSS also showed less strain rate sensitivity compared with the wrought material. Surface morphologies after dynamic tests differed

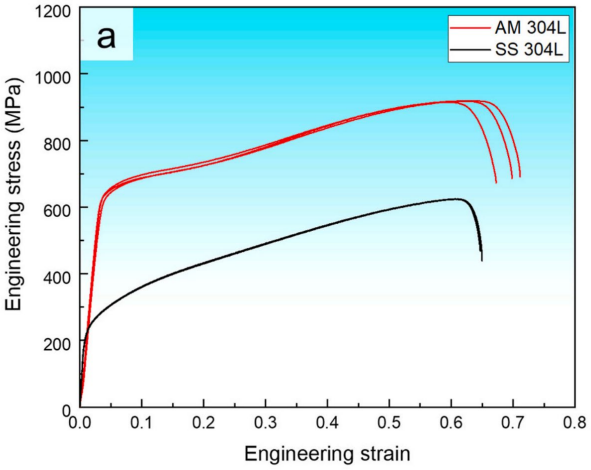

Fig. 9. Engineering curves of stress-strain derived from SS304L and AM304LSS [66].

significantly. This was likely owing to bands of small grains separated by greater grains. This contributed to the surface roughness of the AMed parts [73].

Jeong et al. [17] explored the non-equilibrium microstructures produced by fast cycles of melting and solidification throughout laser-based AMed stainless steels. They focused on the emergence of metastable ultrafine delta-ferrite in DED-fabricated SS304L, which creates a new coherent interface in the austenitic matrix. Through modifying laser scan speeds, they realized that ultrafine δ-ferrite keeps the coherency with the matrix of γ-austenite in the undeformed state. Thus, it makes interactions with dislocations throughout the plastic deformation. This interaction, along with twin intersections and deformation-induced twins, takes part in the outstanding ductility observed in the AM304LSS.

Wang et al. [13] evaluated the impact of processing factors on the mechanical characteristics of SS304L parts manufactured via a laser-based DED process. They manufactured two walls with high linear heat inputs to discover the effect on mechanical properties and microstructure. Their results revealed that the lower linear heat input

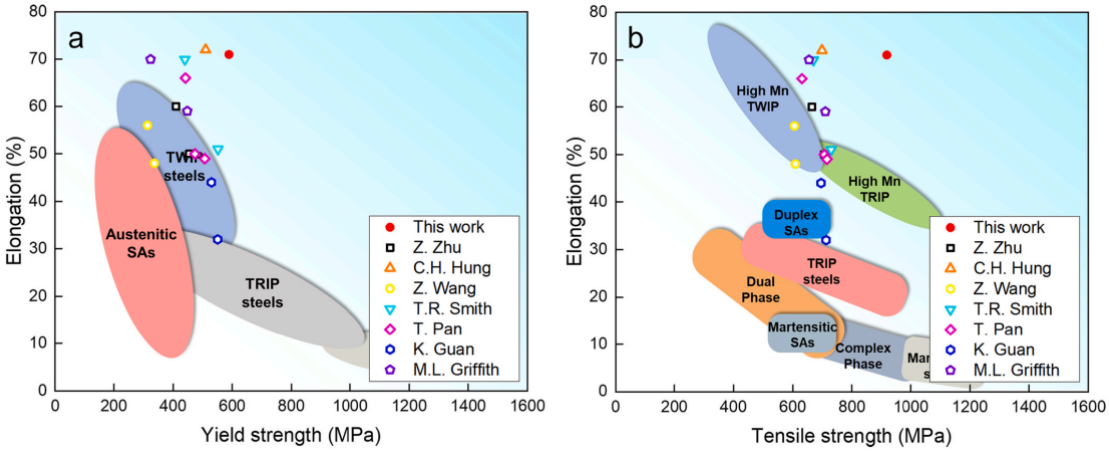

Fig. 10. The tensile strength of the AM304LSS with different steels: a) the YS and b) UTS maps [66].

wall had higher YS, ductility, and UTS, compared to the higher linear heat input wall. This study also noted that the material made by AM had less ductility in the longitudinal direction compared with the transverse direction. Furthermore, the UTSs and ELs of the AMed material were lower than those of the annealed SS304L plate. This was because of the absence of austenite to M-phase transformation, which occurs in the annealed material. This in turn provides substantial macroscopic strain hardening. Chemical analysis showed higher nitrogen content in the AM walls. This leads to the stabilization of the austenitic phase, compared to the annealed plate.

WAAM is known as a favorable technique for fabricating and manufacturing 304L stainless steel components with unique microstructures and tailored mechanical properties. Several studies have investigated the role of processing factors, post-processing techniques, and microstructural characteristics on the performance of WAAM-produced SS304L parts [13].

Gordon et al. [45] explored the FCG behavior of WAAM-produced SS304L and its correlation with the material's microstructure, residual stresses, and texture. Their findings revealed that WAAM-fabricated 304L showed more promising Paris law behavior than conventional wrought SS304L, along with improved FCG resistance and monotonic features. Differences in FCG rate between vertical and horizontal specimens were ascribed to long columnar grains and strong texture, while retained compressive residual stresses positively affected FCG resistance.

Jing et al. [46] adopted the hot-wire method to reduce heat input during WAAM of SS304L. By varying hot-wire currents; they observed a huge reduction in arc heat input. This led to decreased anisotropy, refined grains, and enhanced strength plasticity of the obtained parts.

Elmer et al. [76] investigated the mechanical performance and microstructure of WAAM SS304L parts in different conditions. Their study demonstrated that rolling and heat treatment could modify microstructure and characteristics significantly. Post-processing techniques such as rolling and solution annealing offered means to tailor mechanical properties, with rolled parts exhibiting superior strength and ductility compared to as-built components.

1. In the as-built condition, SS304L walls produced via WAAM showed texture and elastic anisotropy, along with mechanical performance lower than that of conventional annealed stainless steel plates or cast parts.
2. The heat treatment of as-built parts at 1050 °C for 1 hour resulted in some recrystallization, reducing strength. This increased ductility than the as-built condition. Nevertheless, the Young modulus retained the effects of the original texture, remaining at almost half of the polycrystalline value [76].
3. Mechanical rolling of WAAM plates to 40% strain increased YS and UTSs remarkably; comparable to 1/4 to 1/2 hard cold worked 304L stainless steel. Additionally, it exhibited better EL to failure compared to 1/2 hard SS [76].
4. Solution annealing at a temperature of 1050 °C induced microstructural changes dependent on rolling strain. Without rolling strain, the microstructure retained its original features, exhibiting low elastic modulus which is the same as the as-built condition. Nonetheless, with rolling strains of 25% or 40%, recrystallization occurred. This results in isotropic behavior and mechanical properties comparable, or superior, to traditional 304L stainless steel plates and castings [76].

Kemerling et al. [77] evaluated residual stresses in WAAM-produced components and investigated the impact of laser scan strategy and build plate preheating. Their study highlighted the predominance of tensile residual stresses in the directions of x and y, with compressive stresses in the z-direction. Build plate preheating was identified as an effective method for reducing residual stresses, offering insights into stress mitigation strategies for WAAM processes.

5. Conclusions and future insights

AM304LSS is a highly functional and adaptable material that provides significant advantages for a range of industrial applications. In this review, the basic ideas and various AM methods used for fabricating SS304L are emphasized. These methods include DMLS, WAAM, LB-PBF, and SLM. The microstructure and mechanical behavior of the final components are mainly changed by the particular advantages and disadvantages of each process.

The complex interaction between the mechanical performance and microstructure of AM304LSS, and the processing parameters e.g. laser power, scan speed, and particle characteristics, are studied in detail. These parameters need to be optimized to get reliable results, including high corrosion resistance, strength, and ductility. The performance and surface quality of AM304LSS components can be optimized by heat treatment and surface finishing methods as well as process optimization techniques.

This study highlights the advancements in this domain, focusing on the requirement for a deeper comprehension of the interaction between processing parameters and material qualities. Future studies should concentrate on enhancing additive manufacturing procedures, by focusing on innovative post-processing techniques and formulating uniform testing procedures to guarantee the dependability and consistency of AM304LSS parts.

In conclusion, in this review, we aimed to help practitioners, engineers, and academics make the most use of AM304LSS. Taking advantage of the special qualities of the AM process, it is possible to open up new design opportunities and improve the performance of components applicable to important applications. Future developments in this area are quite promising, to open the door to higher-performing, more economical, and efficient metal AM systems.

CRediT authorship contribution statement

Aliasghar Abouchenari: Supervision, Writing – original draft.
Mohamad Javad Jalilpour: Visualization; Writing – review & editing.
Mohammad Reza Ahmadpour Yazdi: Project administration, Writing – original draft.

Data availability

The data underlying this article will be shared on reasonable request to the corresponding author.

Declaration of competing interest

The authors declare no competing interests.

Funding and acknowledgment

The authors received no financial support for this article's research, authorship, and/or publication.

References

[1] E.-J. Kim, C.-M. Lee, D.-H. Kim, The effect of post-processing operations on mechanical characteristics of 304L stainless steel fabricated using laser additive manufacturing, J. Mater. Res. Technol. 15 (2021) 1370–1381. https://doi.org/10.1016/j.jmrt.2021.08.142.

[2] M.-T. Chen, Z. Gong, T. Zhang, W. Zuo, Y. Zhao, et al., Mechanical behavior of austenitic stainless steels produced by wire arc additive manufacturing, Thin-Walled Struct. 196 (2024) 111455. https://doi.org/10.1016/j.tws.2023.111455.

[3] H.E. Sabzi, S.-H. Lim, D.D. Crociata, R. Castellote-Alvarez, M. Simonelli, et al., Genetic design of precipitation-hardening stainless steels for additive manufacturing, Acta Mater. 274 (2024) 120018. https://doi.org/10.1016/j.actamat.2024.120018.

[4] J.O. Milewski, Additive manufacturing metal, the art of the possible, Additive Manufacturing of Metals, Springer, Cham. 258 (2017) 7–33. https://doi.org/10.1007/978-3-319-58205-4_2.

[5] L. Yang, K. Hsu, B. Baughman, D. Godfrey, F. Medina, et al., Additive manufacturing of metals: the technology, materials, design and production, Springer, Cham. (2017). https://doi.org/10.1007/978-3-319-55128-9.

[6] J. Bedmar, A. Riquelme, P. Rodrigo, B. Torres, J. Rams, Comparison of Different Additive Manufacturing Methods for 316L Stainless Steel, Materials. 14 (2021) 6504. https://doi.org/10.3390/ma14216504.

[7] T. DebRoy, H.L. Wei, J.S. Zuback, T. Mukherjee, J.W. Elmer, et al., Additive manufacturing of metallic components – Process, structure and properties, Prog. Mater. Sci. 92 (2018) 112–224. https://doi.org/10.1016/j.pmatsci.2017.10.001.

[8] J. Mazumder, D. Dutta, N. Kikuchi, A. Ghosh, Closed loop direct metal deposition: art to part, Opt. Lasers Eng. 34 (2000) 397–414. https://doi.org/10.1016/S0143-8166(00)00072-5.

[9] S. Bontha, N.W. Klingbeil, P.A. Kobryn, H.L. Fraser, Thermal process maps for predicting solidification microstructure in laser fabrication of thin-wall structures, J. Mater. Process. Technol. 178 (2006) 135–142. https://doi.org/10.1016/j.jmatprotec.2006.03.155.

[10] S. Bontha, N.W. Klingbeil, P.A. Kobryn, H.L. Fraser, Effects of process variables and size-scale on solidification microstructure in beam-based fabrication of bulky 3D structures, Mater. Sci. Eng.: A 513–514 (2009) 311–318. https://doi.org/10.1016/j.msea.2009.02.019.

[11] A. Saboori, A. Aversa, G. Marchese, S. Biamino, M. Lombardi, P. Fino, Microstructure and Mechanical Properties of AISI 316L Produced by Directed Energy Deposition-Based Additive Manufacturing: A Review, Appl. Sci. 10 (2020) 3310. https://doi.org/10.3390/app10093310.

[12] Y. Wang, W. Wen, S. Wu, C. Wang, Z. Yu, et al., Maize Plant Phenotyping: Comparing 3D Laser Scanning, Multi-View Stereo Reconstruction, and 3D Digitizing Estimates, Remote Sens. 11 (2019) 63. https://doi.org/10.3390/rs11010063.

[13] Z. Wang, T.A. Palmer, A.M. Beese, Effect of processing parameters on microstructure and tensile properties of austenitic stainless steel 304L made by directed energy deposition additive manufacturing, Acta Mater. 110 (2016) 226–235. https://doi.org/10.1016/j.actamat.2016.03.019.

[14] L. Gardner, The use of stainless steel in structures, Prog. Struct. Eng. Mater. 7 (2005) 45–55. https://doi.org/10.1002/pse.190.

[15] R.E. Schramm, R.P. Reed, Stacking fault energies of seven commercial austenitic stainless steels, Metall. Trans. A. 6 (1975) 1345–1351. https://doi.org/10.1007/BF02641927.

[16] Z. Zhu, W. Li, Q.B. Nguyen, X. An, W. Lu, et al., Enhanced strength–ductility synergy and transformation-induced plasticity of the selective laser melting fabricated 304L stainless steel, Addit. Manuf. 35 (2020) 101300. https://doi.org/10.1016/j.addma.2020.101300.

[17] J. Jeong, Y. Lee, J.M. Park, D.J. Lee, I. Jeon, et al., Metastable δ-ferrite and twinning-induced plasticity on the strain hardening behavior of directed energy deposition-processed 304L austenitic stainless steel, Addit. Manuf. 47 (2021) 102363. https://doi.org/10.1016/j.addma.2021.102363.

[18] F. Vakili-Tahami, A.H. Daei-Sorkhabi, F.R. Biglari, Experimental Study of the Creep Behaviour of the Cold-Drawn 304L Stainless Steel, Strain. 47 (2011) 111–120. https://doi.org/10.1111/j.1475-1305.2010.00746.x.

[19] K. Guan, Z. Wang, M. Gao, X. Li, X. Zeng, Effects of processing parameters on tensile properties of selective laser melted 304 stainless steel, Mater. Des. 50 (2013) 581–586. https://doi.org/10.1016/j.matdes.2013.03.056.

[20] P. Deng, Q. Peng, E.-H. Han, W. Ke, C. Sun, Z. Jiao, Effect of irradiation on corrosion of 304 nuclear grade stainless steel in simulated PWR primary water, Corros. Sci. 127 (2017) 91–100. https://doi.org/10.1016/j.corsci.2017.08.010.

[21] S.E. Ziemniak, M. Hanson, Corrosion behavior of 304 stainless steel in high temperature, hydrogenated water, Corros. Sci. 44 (2002) 2209–2230. https://doi.org/10.1016/S0010-938X(02)00004-5.

[22] S. Pathak, S. Zulić, J. Kaufman, J. Kopeček, O. Stránský, et al., Post-processing of selective laser melting manufactured SS-304L by laser shock peening, J. Mater. Res. Technol. 19 (2022) 4787–4792. https://doi.org/10.1016/j.jmrt.2022.07.014.

[23] M. Ghayoor, K. Lee, Y. He, C.-h. Chang, B.K. Paul, S. Pasebani, Selective laser melting of 304L stainless steel: Role of volumetric energy density on the microstructure, texture and mechanical properties, Addit. Manuf. 32 (2020) 101011. https://doi.org/10.1016/j.addma.2019.101011.

[24] L. Bait, L. Azzouz, N. Madaoui, N. Saoula, Influence of substrate bias voltage on the properties of TiO2 deposited by radio-frequency magnetron sputtering on 304L for biomaterials applications, Appl. Surf. Sci. 395 (2017) 72–77. https://doi.org/10.1016/j.apsusc.2016.07.101.

[25] H. Yeom, T. Dabney, N. Pocquette, K. Ross, F.E. Pfefferkorn, K. Sridharan, Cold spray deposition of 304L stainless steel to mitigate chloride-induced stress corrosion cracking in canisters for used nuclear fuel storage, J. Nucl. Mater. 538 (2020) 152254. https://doi.org/10.1016/j.jnucmat.2020.152254.

[26] D. D'Andrea, Additive Manufacturing of AISI 316L Stainless Steel: A Review, Metals. 13 (2023) 1370. https://doi.org/10.3390/met13081370.

[27] C.Y. Yap, C.K. Chua, Z.L. Dong, Z.H. Liu, D.Q. Zhang, et al., Review of selective laser melting: Materials and applications, Appl. Phys. Rev. 2 (2015) 041101. https://doi.org/10.1063/1.4935926.

[28] P.K. Gokuldoss, Selective laser melting: Materials and applications, MDPI. (2020). https://doi.org/10.3390/books978-3-03928-579-2.

[29] I. Yadroitsev, I. Yadroitsava, A. Du Plessis, E. MacDonald, Fundamentals of laser powder bed fusion of metals, Elsevier. (2021). https://doi.org/10.1016/C2020-0-01200-4.

[30] I. Yadroitsev, I. Yadroitsava, A. Du Plessis, Basics of laser powder bed fusion, Fundamentals of laser powder bed fusion of metals, Elsevier. (2021) 15–38. https://doi.org/10.1016/B978-0-12-824090-8.00024-X.

[31] W. Liu, H. Wei, A. Liu, Y. Zhang, Multi-index co-evaluation of metal laser direct deposition: An investigation of energy input effect on energy efficiency and mechanical properties of 316l parts, J. Manuf. Process. 76 (2022) 277–290. https://doi.org/10.1016/j.jmapro.2022.02.016.

[32] D. Dev Singh, S. Arjula, A. Raji Reddy, Functionally Graded Materials Manufactured by Direct Energy Deposition: A review, Mater. Today Proc. 47 (2021) 2450–2456. https://doi.org/10.1016/j.matpr.2021.04.536.
[33] M.A. Melia, H.-D.A. Nguyen, J.M. Rodelas, E.J. Schindelholz, Corrosion properties of 304L stainless steel made by directed energy deposition additive manufacturing, Corros. Sci. 152 (2019) 20–30. https://doi.org/10.1016/j.corsci.2019.02.029.
[34] Q. Chao, V. Cruz, S. Thomas, N. Birbilis, P. Collins, et al., On the enhanced corrosion resistance of a selective laser melted austenitic stainless steel, Scr. Mater. 141 (2017) 94–98. https://doi.org/10.1016/j.scriptamat.2017.07.037.
[35] S. Shin, S.-M. Kwon, C. Kim, J. Lee, J. Hwang, H. Kim, Optimization of Direct Energy Deposition of 304L Stainless Steel through Laser Process Parameters, J. Weld. Join. 39 (2021) 182–188. https://doi.org/10.5781/JWJ.2021.39.2.7.
[36] V. Vinoth, S. Sathiyamurthy, U. Natarajan, D. Venkatkumar, J. Prabhakaran, K. Sanjeevi Prakash, Examination of microstructure properties of AISI 316L stainless steel fabricated by wire arc additive manufacturing, Mater. Today Proceed. 66 (2022) 702–706. https://doi.org/10.1016/j.matpr.2022.04.011.
[37] I.Tabernero, A. Paskual, P. Álvarez, A. Suárez, Study on Arc Welding Processes for High Deposition Rate Additive Manufacturing, Proc. CIRP. 68 (2018) 358–362. https://doi.org/10.1016/j.procir.2017.12.095.
[38] M. Sowrirajan, M. Vijayananthan, G. Seenivasagan, J. Sundaresan, A new approach to the fabrication of thin-walled plate component through typical wire arc additive manufacturing, J. Adv. Mech. Sci. 1 (2022) 8–13. https://doi.org/10.5281/zenodo.7046021.
[39] L. Ji, J. Lu, C. Liu, C. Jing, H. Fan, S. Ma, Microstructure and mechanical properties of 304L steel fabricated by arc additive manufacturing, MATEC Web of Conferences, EDP Sci. 128 (2017) 03006. https://doi.org/10.1051/matecconf/201712803006.
[40] Standard Specification for Chromium and Chromium-Nickel Stainless Steel Plate, Sheet, and Strip for Pressure Vessels and for General Applications, ASTM A240/A240M-22a. (2015).
[41] J. Long, M. Wang, W. Zhao, X. Zhang, Y. Wei, W. Ou, High-power wire arc additive manufacturing of stainless steel with active heat management, Sci. Technol. Weld. Join. 27 (2022) 256–264. https://doi.org/10.1080/13621718.2022.2045127.
[42] C.S. Kriewall, A.T. Sutton, M.-C. Leu, J.W. Newkirk, Investigation of Heat-Affected 304L SS Powder and its Effect on Built Parts in Selective Laser Melting, Proceedings of the 27th Annual International Solid Freeform Fabrication Symposium, University of Texas at Austin (2016) 625–639.
[43] C.M. Smudde, C.R. D'Elia, C.W. San Marchi, M.R. Hill, J.C. Gibeling, The influence of residual stress on fatigue crack growth rates of additively manufactured Type 304L stainless steel, Int. J. Fatigue. 162 (2022) 106954. https://doi.org/10.1016/j.ijfatigue.2022.106954.
[44] T.R. Smith, J.D. Sugar, J.M. Schoenung, C. San Marchi, Relationship between manufacturing defects and fatigue properties of additive manufactured austenitic stainless steel, Mater. Sci. Eng: A 765 (2019) 138268. https://doi.org/10.1016/j.msea.2019.138268.
[45] J.V. Gordon, C.V. Haden, H.F. Nied, R.P. Vinci, D.G. Harlow, Fatigue crack growth anisotropy, texture and residual stress in austenitic steel made by wire and arc additive manufacturing, Mater. Sci. Eng: A 724 (2018) 431–438. https://doi.org/10.1016/j.msea.2018.03.075.
[46] C. Jing, Z. Chen, B. Liu, T. Xu, J. Wang, et al., Improving mechanical strength and isotropy for wire-arc additive manufactured 304L stainless steels via controlling arc heat input, Mater. Sci. Eng: A 845 (2022) 143223. https://doi.org/10.1016/j.msea.2022.143223.
[47] M.H. Sehhat, A.T. Sutton, C.-H. Hung, J.W. Newkirk, M.C. Leu, Investigation of Mechanical Properties of Parts Fabricated with Gas- and Water-Atomized 304L Stainless Steel Powder in the Laser Powder Bed Fusion Process, JOM. 74 (2022) 1088–1095. https://doi.org/10.1007/s11837-021-05029-7.
[48] D.-H. Lee, B. Sun, S. Lee, D. Ponge, E.A. Jägle, D. Raabe, Comparative study of hydrogen embrittlement resistance between additively and conventionally manufactured 304L austenitic stainless steels, Mater. Sci. Eng: A 803 (2021) 140499. https://doi.org/10.1016/j.msea.2020.140499.
[49] S. Lee, J.W. Pegues, N. Shamsaei, Fatigue behavior and modeling for additive manufactured 304L stainless steel: The effect of surface roughness, Int. J. Fatigue. 141 (2020) 105856. https://doi.org/10.1016/j.ijfatigue.2020.105856.
[50] C. Hawk, B. Simonds, J. Tanner, R. Pacheco, M. Brand, et al., Laser spot welding of additive manufactured 304L stainless steel, Weld. World. 66 (2022) 895–906. https://doi.org/10.1007/s40194-022-01265-w.
[51] T. Krentz, P. Korinko, A. McWilliams, Fracture and Tensile Characterization of Additively Manufactured Type 300 Series Stainless Steel in the Baseline and Hydrogen Charged Conditions, Pressure Vessels & Piping Conference, ASME. (2022) PVP2022-84723. https://doi.org/10.1115/PVP2022-84723.
[52] A.T. Sutton, C.S. Kriewall, S. Karnati, M.C. Leu, J.W. Newkirk, Characterization of AISI 304L stainless steel powder recycled in the laser powder-bed fusion process, Addit. Manuf. 32 (2020) 100981. https://doi.org/10.1016/j.addma.2019.100981.
[53] N.C. Ferreri, R. Pokharel, V. Livescu, D.W. Brown, M. Knezevic, et al., Effects of heat treatment and build orientation on the evolution of ϵ and α′ martensite and strength during compressive loading of additively manufactured 304L stainless steel, Acta Mater. 195 (2020) 59–70. https://doi.org/10.1016/j.actamat.2020.04.036.
[54] H. Zhang, C. Li, G. Yao, Y. Zhang, Effect of inclusion interface evolution on the thermal stability of cellular substructures in additively manufactured stainless steel, Mater. Sci. Eng: A 841 (2022) 143045. https://doi.org/10.1016/j.msea.2022.143045.
[55] M. Ghayoor, S. Mirzababaei, A. Sittiho, I. Charit, B.K. Paul, S. Pasebani, Thermal stability of additively manufactured austenitic 304L ODS alloy, J. Mater. Sci. Technol. 83 (2021) 208–218. https://doi.org/10.1016/j.jmst.2020.12.033.
[56] P. Deng, H. Yin, M. Song, D. Li, Y. Zheng, et al., On the Thermal Stability of Dislocation Cellular Structures in Additively Manufactured Austenitic Stainless Steels: Roles of Heavy Element Segregation and Stacking Fault Energy, JOM. 72 (2020) 4232–4243. https://doi.org/10.1007/s11837-020-04427-7.
[57] H. Zhang, M. Xu, Z. Liu, C. Li, Y. Zhang, Role of local recrystallization behavior on fatigue performance of SLMed 304L austenitic stainless steels, Mater. Charact. 177 (2021) 111159. https://doi.org/10.1016/j.matchar.2021.111159.
[58] Q.B. Nguyen, Z. Zhu, F.L. Ng, B.W. Chua, S.M.L. Nai, J. Wei, High mechanical strengths and ductility of stainless steel 304L fabricated using selective laser melting, J. Mater. Sci. Technol. 35 (2019) 388–394. https://doi.org/10.1016/j.jmst.2018.10.013.
[59] H. Zhang, M. Xu, P. Kumar, C. Li, Z. Liu, Y. Zhang, Fatigue life prediction model and entropy generation of 304L stainless steel fabricated by selective laser melting, J. Mater. Proc. Technol. 297 (2021) 117279. https://doi.org/10.1016/j.jmatprotec.2021.117279.
[60] L.B. Tomanek, D.S. Stutts, T. Pan, F. Liou, Influence of porosity on the thermal, electrical, and mechanical performance of selective laser melted stainless steel, Addit. Manuf. 39 (2021) 101886. https://doi.org/10.1016/j.addma.2021.101886.
[61] H. Zhang, M. Xu, P. Kumar, C. Li, W. Dai, et al., Enhancement of fatigue resistance of additively manufactured 304L SS by unique heterogeneous microstructure, Virtual Phys. Prototyp. 16 (2021) 125–145. https://doi.org/10.1080/17452759.2021.1881869.
[62] J.G. Kim, J.B. Seol, J.M. Park, H. Sung, S.H. Park, H.S. Kim, Effects of Cell Network Structure on the Strength of Additively Manufactured Stainless Steels, Met. Mater. Int. 27 (2021) 2614–2622. https://doi.org/10.1007/s12540-021-00991-y.

[63] T. Amine, C.S. Kriewall, J.W. Newkirk, Long-Term Effects of Temperature Exposure on SLM 304L Stainless Steel, JOM. 70 (2018) 384–389. https://doi.org/10.1007/s11837-017-2656-4.
[64] C.-H. Hung, A. Sutton, Y. Li, Y. Shen, H.-L. Tsai, M.C. Leu, Enhanced mechanical properties for 304L stainless steel parts fabricated by laser-foil-printing additive manufacturing, J. Manuf. Proc. 45 (2019) 438–446. https://doi.org/10.1016/j.jmapro.2019.07.030.
[65] C.M. Smudde, C.W. San Marchi, M.R. Hill, J.C. Gibeling, Effects of residual stress on orientation dependent fatigue crack growth rates in additively manufactured stainless steel, Int. J. Fatigue. 169 (2023) 107489. https://doi.org/10.1016/j.ijfatigue.2022.107489.
[66] J.-M. Kim, H.-H. Jin, J. Kwon, S.H. Kang, B.-S. Lee, Effects of cellular segregation for high strength and ductility of additively manufactured 304L stainless steel, Mater. Charact. 194 (2022) 112364. https://doi.org/10.1016/j.matchar.2022.112364.
[67] J. Talonen, H. Hänninen, P. Nenonen, G. Pape, Effect of strain rate on the strain-induced γ → α′-martensite transformation and mechanical properties of austenitic stainless steels, Metal. Mater.Trans. A. 36 (2005) 421–432. https://doi.org/10.1007/s11661-005-0313-y.
[68] P. Gargarella, C.S. Kiminami, E.M. Mazzer, R.D. Cava, L.A. Basilio, et al., Phase Formation, Thermal Stability and Mechanical Properties of a Cu-Al-Ni-Mn Shape Memory Alloy Prepared by Selective Laser Melting, Mater. Res. 18 (2015) 35–38. https://doi.org/10.1590/1516-1439.338914.
[69] T. Pan, S. Karnati, Y. Zhang, X. Zhang, C.-H. Hung, et al., Experiment characterization and formulation estimation of tensile properties for selective laser melting manufactured 304L stainless steel, Mater. Sci. Eng: A 798 (2020) 140086. https://doi.org/10.1016/j.msea.2020.140086.
[70] P. Shi, W. Ren, T. Zheng, Z. Ren, X. Hou, et al., Enhanced strength–ductility synergy in ultrafine-grained eutectic high-entropy alloys by inheriting microstructural lamellae, Nat. Commun. 10 (2019) 489. https://doi.org/10.1038/s41467-019-08460-2.
[71] A. McWilliams, M. Morgan, P. Korinko, Hydrogen Effects on Fracture Toughness of Additively Manufactured Type 304L Stainless Steel, ASME 2019 Pressure Vessels & Piping Conference. (2019).
[72] T.R. Smith, C. San Marchi, J.D. Sugar, D.K. Balch, Effects of Extreme Hydrogen Environments on the Fracture and Fatigue Behavior of Additively Manufactured Stainless Steels, ASME 2019 Pressure Vessels & Piping Conference. (2019).
[73] Z. Wang, A.M. Beese, Effect of chemistry on martensitic phase transformation kinetics and resulting properties of additively manufactured stainless steel, Acta Mater. 131 (2017) 410–422. https://doi.org/10.1016/j.actamat.2017.04.022.
[74] D.W. Brown, D.P. Adams, L. Balogh, J.S. Carpenter, B. Clausen, et al., Using In Situ Neutron Diffraction to Isolate Specific Features of Additively Manufactured Microstructures in 304L Stainless Steel and Identify Their Effects on Macroscopic Strength, Metall. Mater. Trans. A 50 (2019) 3399–3413. https://doi.org/10.1007/s11661-019-05240-x.
[75] E. Nishida, B. Song, M. Maguire, D. Adams, J. Carroll, et al., Dynamic compressive response of wrought and additive manufactured 304L stainless steels, EPJ Web of Conferences. 94 (2015) 01001. https://doi.org/10.1051/epjconf/20159401001.
[76] J.W. Elmer, G. Gibbs, Mechanical rolling and annealing of wire-arc additively manufactured stainless steel plates, Sci. Technol. Weld. Join. 27 (2022) 14–21. https://doi.org/10.1080/13621718.2021.1996003.
[77] B. Kemerling, J.C. Lippold, C.M. Fancher, J. Bunn, Residual stress evaluation of components produced via direct metal laser sintering, Weld. World. 62 (2018) 663–674. https://doi.org/10.1007/s40194-018-0572-z.